We are IntechOpen, the world's leading publisher of Open Access books Built by scientists, for scientists

6,900
Open access books available

186,000
International authors and editors

200M
Downloads

Our authors are among the

154
Countries delivered to

TOP 1%
most cited scientists

12.2%
Contributors from top 500 universities

WEB OF SCIENCE™

Selection of our books indexed in the Book Citation Index in Web of Science™ Core Collection (BKCI)

Interested in publishing with us?
Contact book.department@intechopen.com

Numbers displayed above are based on latest data collected.
For more information visit www.intechopen.com

Chapter 5

Trajectory Tracking Control of Parallel Manipulator with Integral Manifold and Observer

Zhengsheng Chen

Additional information is available at the end of the chapter

http://dx.doi.org/10.5772/intechopen.80375

Abstract

In view of the problem that notable flexible displacement will occur for parallel manipulators when operating at high speed, the composite controller based on the integral manifold and high-gain observer is proposed for trajectory tracking and the 3RRR parallel manipulator is taken as the object. Based on the stiffness matrix, the small variable is introduced to decompose the rigid-flexible coupling dynamic model into slow and fast subsystem. For the slow subsystem, the backstepping control is applied for rigid motion tracking. In order to account for the links' flexible displacement the corrective torque is deduced, and the compensation for the flexible displacement is realized. For the fast subsystem, the sliding mode control is utilized to suppress the vibration. The high-gain observer is designed to avoid the measurement of the curvature rate of flexible links. Also, the stability of the overall system is proven with the Lyapunov stability theorem and the upper bound of the small variable is obtained. At last, the proposed composite controller together with the singular perturbation control and the rigid body model-based backstepping control are simulated, and vibration suppression and tracking performances are compared to validate the proposed control scheme.

Keywords: parallel manipulator, integral manifold, high-gain observer, composite control, sliding mode control, backstepping control, vibration suppression

1. Introduction

Parallel manipulators (PMs) possess advantages of high precision, high stiffness, and large load-to-weight ratio; they have attracted wide attention and have been widely used in industries such as high-speed handling, motion simulation, and electronic manufacturing [1]. However, in order to increase efficiency, PMs are increasingly used in high-speed and heavy-duty operations. In order to reduce costs and energy consumption, the lightweight design of the mechanical body

IntechOpen

© 2018 The Author(s). Licensee IntechOpen. This chapter is distributed under the terms of the Creative Commons Attribution License (http://creativecommons.org/licenses/by/3.0), which permits unrestricted use, distribution, and reproduction in any medium, provided the original work is properly cited. CC BY

will be the inevitable choice. However, in the high-speed or heavy-duty application, the lightweight mechanical body will produce significant elastic deformation and vibration. Therefore, the end-effector's movement consists of the rigid-body motion and the elastic displacement caused by elastic deformation and vibration. Using conventional control methods for rigid-body manipulators will not guarantee good tracking accuracy of flexible manipulator's end-effector. Therefore, it is of great significance to improve the tracking accuracy of high-speed lightweight PMs by considering the flexibility of members to establish the dynamic model for rigid-flexible coupling and carrying out research on high-precision control algorithms.

Many scholars have conducted extensive and in-depth studies on modeling methods for manipulators with flexible links. Dwivedy et al. [2] reviewed the dynamic modeling of robots with flexible links. Due to the presence of link flexibility, the system will exhibit nonminimum phase characteristics when selecting the end-effector of the manipulator as the output. The literature [3–5] redefines the output of the manipulator's end position by taking the link elasticity into account, and uses the control algorithm for the rigid-body manipulator to control the new output; however, this method can only realize the point-to-point position control and cannot guarantee tracking control of the end trajectory [6]. The singular perturbation method is another effective method to deal with the nonminimum phase characteristics of manipulators with elastic links. The small parameters are introduced to reduce the order of rigid-flexible coupling models, which are decomposed into two subsystems, the fast and the slow, and two subcontrollers are designed using compound control algorithm. The controller of the system realizes the control of the rigid body motion and the rapid suppression of the elastic vibration. However, as the deformation increases, the singularity perturbation algorithm shows a deficiency and the algorithm cannot compensate for the elastic displacement [7–9]. Khorasani [10] proposed an integral manifold method by high-order approximation of fast subsystem variables, which greatly improved the vibration suppression effect. By introducing the elastic displacement into the end of the manipulator and designing the corrective torque, Moallem et al. [11] realized the trajectory tracking precision control and vibration suppression of the two-degree-of-freedom serial robot. Based on the above method, Fotouhi et al. [12–16] studied the trajectory tracking control of the flexible joint robot, the flexible robot with the single link, the rigid-flexible hybrid robot, and the two-bar flexible robot by simplifying the selection of correction moments, and show good results.

Due to the existence of the closed-chain structure, the dynamic model of PMs is complex when considering the flexibility of the links. Therefore, the research on the vibration suppression and trajectory tracking control is very limited. Zhang et al. [7] used assumption mode method and Lagrange equation to model 3PRR PMs with flexible passive links, and adopted singular perturbation compound control to suppress vibration. However, the influence of the elastic displacement of the links on the moving platform is not considered in the model, and the elastic displacement compensation and the rate of change of the elastic links are not processed when the algorithm is designed. Therefore, the trajectory tracking effect needs to be improved. Existing research has not yet been found for the above issues. In the research of trajectory tracking control based on integral manifold, no relevant research has been found for PMs. The control algorithms for the slow subsystem in the existing research are feedback linearization methods, and the fast subsystem is PD control or pole placement. In order to taking into accounts of the elastic deformation and vibration of high-speed PMs due to the flexibility of

http://dx.doi.org/10.5772/intechopen.80375

links and improve the tracking accuracy and dynamic performance, this chapter introduces the integral manifold based on the rigid-flexible coupling model of the 3RRR PM, the hypothesis of small deformation and the velocity mapping in the previous paper [17], and the high-order rigid-flexible coupling model is transformed into two subsystems, then a composite control algorithm based on sliding mode variable structure control and backstepping control is proposed. At the same time, a high-gain observer is introduced to the curvature rate caused by the flexibility. Finally, simulation studies are conducted to verify the feasibility of the algorithm.

2. The dynamic model of the 3RRR PM

The structure of the 3RRR parallel manipulator was shown in **Figure 1**, which consists of three branches, and each branch composed of one active link and passive link, the end of which is the moving platform. The coordinates and the parameters are given in **Figure 2**, $O-XY$ and $G-x_Gy_G$ are the coordinate frames attached with the base and moving platform, with O and G as the origin, respectively. θ_i and β_i are the angles of the active and passive links, $i=1,2,3$, the position and attitude of the moving platform are depicted as $\boldsymbol{\eta}=\begin{bmatrix}x & y & \phi\end{bmatrix}^{\mathrm{T}}$ in the base frame.

According to our previously published paper [17], the flexibility of passive links can be neglected, so only the deformation of active links is considered here, which can be expressed as $\delta_i=\sum_{k=1}^{n}\alpha_i^k m_i^k$, $i=1,2,3$, where α_i^k and m_i^k are the shape function and the curvature of the kth point in the ith active link, respectively, where $k=1$. According to [17], after ignoring the deformation of the passive links and adding the parameters of the motors and reducers, the dynamic model of the PM can be expressed as:

$$\begin{bmatrix}(\boldsymbol{M}_{11})_0+(\boldsymbol{M}_{11})_1 & \boldsymbol{M}_{12}\\ \boldsymbol{M}_{12}^{\mathrm{T}} & \boldsymbol{M}_{22}\end{bmatrix}\begin{bmatrix}\ddot{\boldsymbol{\eta}}\\ \ddot{\boldsymbol{m}}\end{bmatrix}+\begin{bmatrix}\boldsymbol{0} & \boldsymbol{0}\\ \boldsymbol{0} & \boldsymbol{K}\end{bmatrix}\begin{bmatrix}\boldsymbol{\eta}\\ \boldsymbol{m}\end{bmatrix}+\begin{bmatrix}(\boldsymbol{f}_1)_0+M_{f1}\boldsymbol{m}+M_{f2}\dot{\boldsymbol{m}}\\ (\boldsymbol{f}_2)_0+M_{f3}\dot{\boldsymbol{m}}\end{bmatrix}=\begin{bmatrix}\boldsymbol{J}_{p\theta}^{\mathrm{T}}\boldsymbol{\tau}\\ \boldsymbol{0}\end{bmatrix} \quad (1)$$

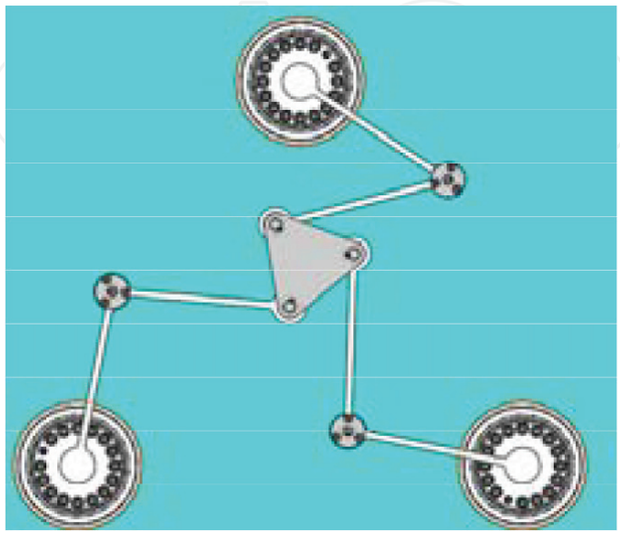

Figure 1. The 3RRR PM.

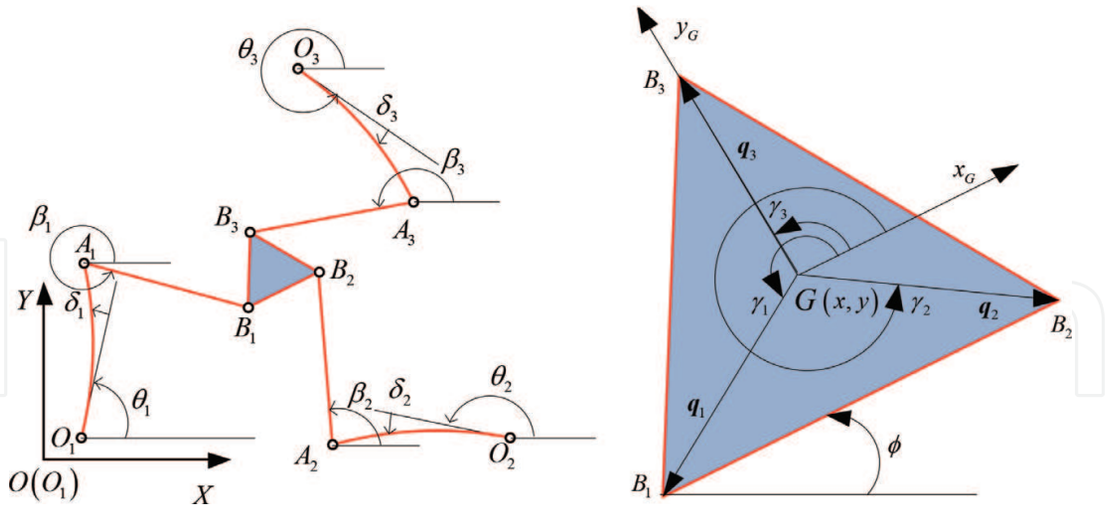

Figure 2. Coordinates of the 3RRR PM.

where J_m and J_g are the moment of inertia of the motor and the reducer, and $\boldsymbol{K} = \mathbf{diag}([k_s, k_s, k_s])$ is the stiffness matrix, while k_s and i_g are the link's stiffness and the reduction ratio, respectively, $\boldsymbol{\tau}$ represents the driving torque, $\left(\boldsymbol{M}'_{11}\right)_0$ and $\left(\boldsymbol{f}'_1\right)_0$ are the mass matrix and quadratic terms in the dynamic equation derived from [17], while the item corresponding to $\boldsymbol{m}$ is neglected.

3. Integral manifold-based model reduction of the high-speed PM

From the dynamic model (1), the state variables are defined as below [15],

$$\begin{cases} \boldsymbol{X}_1 = \boldsymbol{\eta}, \boldsymbol{X}_2 = \dot{\boldsymbol{\eta}} \\ \boldsymbol{z}_1 = \boldsymbol{m}/\varepsilon^2, \boldsymbol{z}_2 = \dot{\boldsymbol{m}}/\varepsilon \end{cases} \tag{2}$$

where $\boldsymbol{z} = [\boldsymbol{z}_1\ \boldsymbol{z}_2]^{\mathrm{T}}$ and $\boldsymbol{X} = [\boldsymbol{X}_1\ \boldsymbol{X}_2]^{\mathrm{T}}$ are state variables of the slow subsystem, $\varepsilon \in \boldsymbol{R}$ is the small parameter larger than zero, which are used for subsequent model reduction and time scale transformation. From the state variables (2) and the system Eq. (1), the state equation of the perturbed form can be expressed as:

$$\begin{cases} \dot{\boldsymbol{X}}_1 = \boldsymbol{X}_2, \\ \dot{\boldsymbol{X}}_2 = \boldsymbol{J}_{11}\boldsymbol{J}_{p\theta}^{\mathrm{T}}\boldsymbol{\tau} - \boldsymbol{J}_{11}\boldsymbol{f}_1 - \boldsymbol{J}_{12}\boldsymbol{f}_2 - \boldsymbol{J}_{12}\tilde{k}\boldsymbol{z}_1; \end{cases} \tag{3}$$

$$\begin{cases} \varepsilon\dot{\boldsymbol{z}}_1 = \boldsymbol{z}_2, \\ \varepsilon\dot{\boldsymbol{z}}_2 = \boldsymbol{J}_{12}^{\mathrm{T}}\boldsymbol{J}_{p\theta}^{\mathrm{T}}\boldsymbol{\tau} - \boldsymbol{J}_{12}^{\mathrm{T}}\boldsymbol{f}_1 - \boldsymbol{J}_{22}\boldsymbol{f}_2 - \boldsymbol{J}_{22}\tilde{k}\boldsymbol{z}_1. \end{cases} \tag{4}$$

where $\tilde{k} = k_s\varepsilon^2$ is the stiffness coefficient, $\boldsymbol{J} = \begin{bmatrix} \boldsymbol{J}_{11} & \boldsymbol{J}_{12}; & \boldsymbol{J}_{12}^{\mathrm{T}} & \boldsymbol{J}_{22} \end{bmatrix}$ is the inverse matrix of the mass matrix $\boldsymbol{M}$.

For Eq. (4), the integral manifold is defined as [15, 18],

$$\boldsymbol{z}(t^*,\varepsilon)=\boldsymbol{h}(\boldsymbol{X}_1(t^*,\varepsilon),\boldsymbol{X}_2(t^*,\varepsilon),\boldsymbol{\tau}(t^*),\varepsilon)\Rightarrow\boldsymbol{z}(t,\varepsilon)=\boldsymbol{h}^a(\boldsymbol{X}_1(t,\varepsilon),\boldsymbol{X}_2(t,\varepsilon),\boldsymbol{\tau}(t),\varepsilon) \tag{5}$$

Eq. (5) can be interpreted that if the fast subsystem variables arrive at the integral manifold trajectory at the moment t^*, then for the moment $\forall t > t^*$, the variable will always remain on the manifold trajectory. In order to ensure the above conditions valid, the additional control variables are added in the control system.

Due to the small variable ε close to 0, the integral manifold $\boldsymbol{h}$ and the moment $\boldsymbol{\tau}$ are all functions of ε, Taylor expansion of the above variables is available as,

$$\begin{cases}\boldsymbol{h}_1^a\approx\boldsymbol{h}_1=\boldsymbol{h}_{10}+\varepsilon\boldsymbol{h}_{11}(\boldsymbol{X}_1,\boldsymbol{X}_2,t)+\ldots+\varepsilon^p\boldsymbol{h}_{1p}(\boldsymbol{X}_1,\boldsymbol{X}_2,t)\\ \boldsymbol{h}_2^a\approx\boldsymbol{h}_2=\boldsymbol{h}_{20}+\varepsilon\boldsymbol{h}_{21}(\boldsymbol{X}_1,\boldsymbol{X}_2,t)+\ldots+\varepsilon^p\boldsymbol{h}_{2p}(\boldsymbol{X}_1,\boldsymbol{X}_2,t)\\ \boldsymbol{\tau}\approx\boldsymbol{\tau}_0+\varepsilon\boldsymbol{\tau}_1(\boldsymbol{X}_1,\boldsymbol{X}_2,t)+\ldots+\varepsilon^p\boldsymbol{\tau}_p(\boldsymbol{X}_1,\boldsymbol{X}_2,t).\end{cases} \tag{6}$$

where $\boldsymbol{h}_1$ and $\boldsymbol{h}_2$ are the approximations of $\boldsymbol{h}_1{}^a$and $\boldsymbol{h}_2{}^a$, and $\boldsymbol{h}_{ij}=\frac{\partial^j h_i^a}{j!\partial\varepsilon^j}|_{\varepsilon=0}$ is the derivative of the integral manifold with respect to the small variable ε, while $i=1,2\ \ j=0,1,2,\ldots p$, and $p\in N^+$ is the approximation order. Since the elastic displacement of the link is ε^2 times of the state variable $\boldsymbol{z}$ of the fast subsystem, so p should be at least 2 when the elastic displacement can be accounted in the end trajectory, the p is selected 2 here.

The inverse matrix of the mass matrix, the Coriolis force and the centrifugal force terms are functions of the small variable ε, the Taylor expansion of the inverse matrix about ε can be expressed as,

$$\begin{cases}\boldsymbol{J}_{11}=(\boldsymbol{J}_{11})_0,\boldsymbol{J}_{12}=(\boldsymbol{J}_{12})_0\\ \boldsymbol{J}_{22}=(\boldsymbol{J}_{22})_0+(\boldsymbol{J}_{22})_2\varepsilon^2/2\end{cases} \tag{7}$$

The centrifugal and inertial force after the expansion of Eq. (1) can be expressed as,

$$\begin{cases}\boldsymbol{f}_1=(\boldsymbol{f}_1)_0+\left((\boldsymbol{f}_1)_{20}\boldsymbol{h}_{10}+(\boldsymbol{f}_1)_{21}\dot{\boldsymbol{h}}_{10}\right)\varepsilon^2/2,\\ \boldsymbol{f}_2=(\boldsymbol{f}_2)_0+\varepsilon^2(\boldsymbol{f}_2)_{21}\dot{\boldsymbol{h}}_{10}/2.\end{cases} \tag{8}$$

Substituting Eqs. (6) through (8) into Eq. (4), we can obtain,

$$\begin{cases}\boldsymbol{h}_{10}=\left(\boldsymbol{J}_{22}\tilde{k}\right)_0^{-1}\left(\boldsymbol{J}_{12}^{\mathrm{T}}\boldsymbol{J}_{p\theta}^{\mathrm{T}}\boldsymbol{\tau}_0-\boldsymbol{J}_{12}^{\mathrm{T}}(\boldsymbol{f}_1)_0-(\boldsymbol{J}_{22})_0(\boldsymbol{f}_2)_0\right),\\ \boldsymbol{h}_{11}=\left(\boldsymbol{J}_{22}\tilde{k}\right)_0^{-1}\left(\boldsymbol{J}_{12}^{\mathrm{T}}\boldsymbol{J}_{p\theta}^{\mathrm{T}}\boldsymbol{\tau}_1-\dot{\boldsymbol{h}}_{20}\right),\\ \boldsymbol{h}_{12}=\left(\boldsymbol{J}_{22}\tilde{k}\right)_0^{-1}\left(\boldsymbol{J}_{12}^{\mathrm{T}}\boldsymbol{J}_{p\theta}^{\mathrm{T}}\boldsymbol{\tau}_2-\dot{\boldsymbol{h}}_{21}-\boldsymbol{J}_{12}^{\mathrm{T}}\left((\boldsymbol{f}_1)_{20}\boldsymbol{h}_{10}+(\boldsymbol{f}_1)_{21}\dot{\boldsymbol{h}}_{10}\right)/2-\right)(\boldsymbol{J}_{22})_2\left((\boldsymbol{f}_2)_0+\boldsymbol{h}_{10}\right)/2-(\boldsymbol{J}_{22})_0(\boldsymbol{f}_2)_{21}\dot{\boldsymbol{h}}_{10}/2\Big),\\ \boldsymbol{h}_{20}=0,\boldsymbol{h}_{21}=\dot{\boldsymbol{h}}_{10},\boldsymbol{h}_{22}=\dot{\boldsymbol{h}}_{11}.\end{cases} \tag{9}$$

When the flexibility of the links is ignored, the small variable $\varepsilon=0$ is valid. Substituting $\boldsymbol{h}_1$ into Eq. (3), the differential equation of the slow subsystem can be obtained as,

$$\begin{cases} \dot{\overline{X}}_1 = \overline{X}_2 \\ \dot{\overline{X}}_2 = (\boldsymbol{M}_{11})_0^{-1} \boldsymbol{J}_{p\theta}^{\mathrm{T}} \boldsymbol{\tau}_0 - (\boldsymbol{M})_{110}^{-1} (\boldsymbol{f}_1)_0 \end{cases} \tag{10}$$

where $\overline{X}_1$ and $\overline{X}_2$ represent variables of the slow subsystem, for the convenience of description, $\overline{X}_1$ and $\overline{X}_2$ are replaced by X_1 and X_2 in the following expressions,

According to the integral manifold, the deviation of the fast subsystem variable can be expressed as,

$$\begin{cases} \boldsymbol{X}_{f1} = \boldsymbol{z}_1 - \boldsymbol{h}_{10} - \varepsilon \boldsymbol{h}_{11} - \varepsilon^2 \boldsymbol{h}_{12} \\ \boldsymbol{X}_{f2} = \boldsymbol{z}_2 - \boldsymbol{h}_{20} - \varepsilon \boldsymbol{h}_{21} - \varepsilon^2 \boldsymbol{h}_{22} \end{cases} \tag{11}$$

Multiply the Eq. (11) with ε, derive and substitute it into Eq. (6). According to Eq. (9), the fast subsystem equation can be obtained by substituting $\boldsymbol{h}_{ij}$,

$$\begin{cases} \varepsilon \dot{\boldsymbol{X}}_{f1} = \boldsymbol{X}_{f2}, \\ \varepsilon \dot{\boldsymbol{X}}_{f2} = \boldsymbol{J}_{12}^{\mathrm{T}} \boldsymbol{J}_{p\theta}^{\mathrm{T}} \boldsymbol{\tau}_f - (\boldsymbol{J}_{22})_0 \tilde{k} \boldsymbol{X}_{f1} - \varepsilon^2 \left((\boldsymbol{J}_{22})_2 + \boldsymbol{J}_{12}^{\mathrm{T}} (\boldsymbol{f}_1)_{20} \right) \boldsymbol{X}_{f1}/2 - \\ \qquad \varepsilon \left(\boldsymbol{J}_{12}^{\mathrm{T}} (\boldsymbol{f}_1)_{21} + (\boldsymbol{J}_{22})_0 (\boldsymbol{f}_2)_{21} \right) \boldsymbol{X}_{f2}/2. \end{cases} \tag{12}$$

For the slow and fast subsystems represented by Eqs. (10) and (12), the composite control algorithm is designed as shown in **Figure 3**. For the slow subsystem, the backstepping control is used to achieve the tracking control of the rigid body motion. At the same time, according to the velocity mapping relationship, the mapping relationship between the elastic deformation of the links and the elastic displacement of the moving platform is established. The motion of the moving platform is obtained according to the rigid-body motion and the elastic displacement, and the elastic torque compensation is realized by designing the correction torque $\boldsymbol{\tau}_1$ and $\boldsymbol{\tau}_2$. For fast subsystems, the sliding mode control is used to ensure the manifold valid. Considering the difficulty of measuring the rate of curvature change of the links, a high-gain observer will be designed to estimate the rate of curvature change based on the curvature value. The algorithm design will be based on the control structure shown in **Figure 3**.

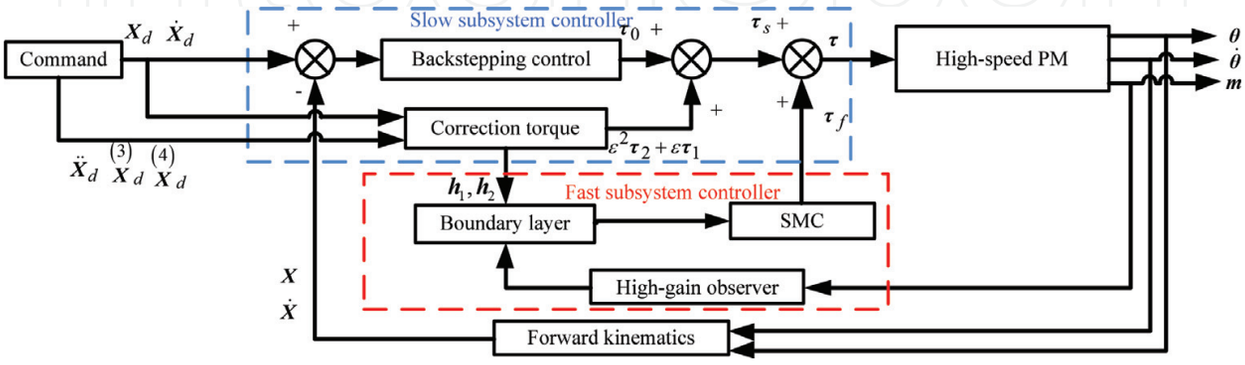

Figure 3. Scheme of the controller.

http://dx.doi.org/10.5772/intechopen.80375

4. The backstepping algorithm-based slow subsystem control

The backstepping control is a recursive control algorithm for complex nonlinear systems. The original system is decomposed into subsystems that do not exceed the system order. The control design is realized by establishing Lyapunov functions step by step for each subsystem, and the stability of the system is ensured [19]. First, define the position error as,

$$\boldsymbol{e}_1 = \boldsymbol{X}_1 - \boldsymbol{X}_d \tag{13}$$

where $\boldsymbol{X}_d$ is the command signal, define the amount of virtual control as,

$$\upsilon_1 = -c_1\boldsymbol{e}_1 + \dot{\boldsymbol{X}}_d \tag{14}$$

where c_1 is a constant greater than zero and the velocity error $\boldsymbol{e}_2$ can be defined as,

$$\boldsymbol{e}_2 = \boldsymbol{X}_2 - \upsilon_1 . \tag{15}$$

Based on the position error, define the Lyapunov function as,

$$\boldsymbol{V}_1 = 1/2\boldsymbol{e}_1^{\mathrm{T}}\boldsymbol{e}_1 . \tag{16}$$

Deriving Eq. (16) can be obtained,

$$\dot{\boldsymbol{V}}_1 = \boldsymbol{e}_1^{\mathrm{T}}\dot{\boldsymbol{e}}_1 = -c_1\boldsymbol{e}_1^{\mathrm{T}}\boldsymbol{e}_1 + \boldsymbol{e}_1^{\mathrm{T}}\boldsymbol{e}_2 . \tag{17}$$

According to the velocity error (15) in conjunction with Eq. (17), the Lyapunov function is defined as,

$$\boldsymbol{V}_2 = \boldsymbol{V}_1 + 1/2\boldsymbol{e}_2^{\mathrm{T}}\boldsymbol{e}_2 = 1/2\boldsymbol{e}_1^{\mathrm{T}}\boldsymbol{e}_1 + 1/2\boldsymbol{e}_2^{\mathrm{T}}\boldsymbol{e}_2 . \tag{18}$$

Deriving the above formula and substituting the relevant parameters, the derivative of the Lyapunov function can be expressed as,

$$\dot{\boldsymbol{V}}_2 = -c_1\boldsymbol{e}_1^{\mathrm{T}}\boldsymbol{e}_1 + \boldsymbol{e}_1^{\mathrm{T}}\boldsymbol{e}_2 + \boldsymbol{e}_2^{\mathrm{T}}\dot{\boldsymbol{e}}_2 = \boldsymbol{e}_2^{T}\left((\boldsymbol{M}_{11})_0^{-1}\boldsymbol{J}_{p\theta}^{\mathrm{T}}\boldsymbol{\tau}_0 - (\boldsymbol{M}_{11})_0^{-1}(\boldsymbol{f}_1)_0 + c_1\dot{\boldsymbol{e}}_1 - \ddot{\boldsymbol{X}}_d\right) - c_1\boldsymbol{e}_1^{\mathrm{T}}\boldsymbol{e}_1 + \boldsymbol{e}_1^{\mathrm{T}}\boldsymbol{e}_2 \tag{19}$$

According to Eq. (19), the control torque of the slow subsystem is

$$\begin{aligned}\boldsymbol{\tau}_0 &= \left(\boldsymbol{J}_{p\theta}^{\mathrm{T}}\right)^{-1}\left((\boldsymbol{f}_1)_0 + (\boldsymbol{M}_{11})_0(-c_1\dot{\boldsymbol{e}}_1 + \ddot{\boldsymbol{X}}_d - c_2\boldsymbol{e}_2 - \boldsymbol{e}_1)\right) \\ &= \left(\boldsymbol{J}_{p\theta}^{\mathrm{T}}\right)^{-1}\left((\boldsymbol{f}_1)_0 + (\boldsymbol{M}_{11})_0(\ddot{\boldsymbol{X}}_d - (c_1 + c_2)\dot{\boldsymbol{e}}_1 - (c_1c_2 + 1)\boldsymbol{e}_1)\right)\end{aligned} \tag{20}$$

where c_2 is a positive real number, and substitute Eq. (20) into Eq. (19), the derivative of the Lyapunov function of the slow subsystem can be expressed as:

$$\dot{\boldsymbol{V}} = -c_1\boldsymbol{e}_1^{\mathrm{T}}\boldsymbol{e}_1 + c_2\boldsymbol{e}_2^{\mathrm{T}}\boldsymbol{e}_2 \le 0 \tag{21}$$

Therefore, according to the Lyapunov stability principle, the slow subsystem is stable with the torque $\boldsymbol{\tau}_0$. Due to the existence of the elasticity, the end position of the PM can be expressed as:

$$\boldsymbol{r} = \boldsymbol{X}_1 + \boldsymbol{f}_3(\boldsymbol{\eta}, \boldsymbol{h}_{10}, \boldsymbol{h}_{11}, \boldsymbol{h}_{12}, \varepsilon). \tag{22}$$

where $\boldsymbol{f}_3$ is the elastic displacement of the center G of the moving platform induced by the elastic deformation and vibration of the links, which is the elastic displacement of the end-effector of the moving platform.

According to the velocity mapping relationship, the acceleration of the moving platform generated by the elastic motion can be expressed as,

$$\ddot{\boldsymbol{f}}_3 = \varepsilon^2 \boldsymbol{J}_{p\theta}^{-1} \boldsymbol{\phi}_l (\boldsymbol{h}_{10} + \varepsilon \boldsymbol{h}_{11} + \varepsilon^2 \boldsymbol{h}_{12})/l_1 + \varepsilon^2 \dot{\overline{\boldsymbol{J}_{p\theta}^{-1}}} \boldsymbol{\phi}_l \left(\dot{\boldsymbol{h}}_{10} + \varepsilon \dot{\boldsymbol{h}}_{11} + \varepsilon^2 \dot{\boldsymbol{h}}_{12}\right)/l_1. \tag{23}$$

where $\dot{\overline{\boldsymbol{J}_{p\theta}^{-1}}}$ is the time derivative of $\boldsymbol{J}_{p\theta}^{-1}$.

The flexibility examined in this chapter is within a small deformation range, and the elastic displacement $\boldsymbol{f}_3$ of the end-effector of the moving platform due to the elastic displacement of the rod can be simplified as,

$$\boldsymbol{f}_3 = \varepsilon^2 \boldsymbol{J}_{p\theta}^{-1} \boldsymbol{\phi}_l \left(\boldsymbol{h}_{10} + \varepsilon \boldsymbol{h}_{11} + \varepsilon^2 \boldsymbol{h}_{12}\right)/l_1. \tag{24}$$

Make the second derivative of Eq. (22), when considering the rigid-flexible coupling motion, the acceleration of the end-effector of the moving platform can be expressed as,

$$\begin{aligned} \ddot{\boldsymbol{r}} = {} & \ddot{\boldsymbol{X}}_d + (c_1 + c_2)(\dot{\boldsymbol{X}}_d - \dot{\boldsymbol{\eta}}) + (c_1 c_2 + 1)(\boldsymbol{X}_d - \boldsymbol{\eta}) + \boldsymbol{M}_{11}^{-1} \boldsymbol{J}_{p\theta}^{\mathrm{T}} (\varepsilon \boldsymbol{\tau}_1 + \varepsilon^2 \boldsymbol{\tau}_2) \\ & + \varepsilon^2 \left(\boldsymbol{J}_{p\theta}^{-1} \boldsymbol{\phi}_l \ddot{\boldsymbol{h}}_{10} + \dot{\overline{\boldsymbol{J}_{p\theta}^{-1}}} \boldsymbol{\phi}_l \dot{\boldsymbol{h}}_{10} \right)/l_1 - \boldsymbol{M}_{11}^{-1} \left((\boldsymbol{f}_1)_{20} \boldsymbol{h}_{10} + (\boldsymbol{f}_1)_{21} \dot{\boldsymbol{h}}_{10} \right) \varepsilon^2/2 \\ & + \boldsymbol{J}_{12} (\boldsymbol{J}_{22})_0^{-1} (\boldsymbol{J}_{22})_2 \left((\boldsymbol{f}_2)_0 + \boldsymbol{h}_{10} \right) \varepsilon^2/2 + \boldsymbol{J}_{12} (\boldsymbol{J}_{22})_0^{-1} \ddot{\boldsymbol{h}}_{10} \varepsilon^2 + \boldsymbol{J}_{12} (\boldsymbol{f}_2)_{21} \dot{\boldsymbol{h}}_{10} \varepsilon^2/2. \end{aligned} \tag{25}$$

Defining the position error $\boldsymbol{e}_3 = \boldsymbol{X}_d - \boldsymbol{r}$ and velocity error $\boldsymbol{e}_4 = \dot{\boldsymbol{e}}_3$ of the end-effector of the moving platform, Eq. (25) can be transformed as,

$$\begin{cases} \dot{\boldsymbol{e}}_3 = \boldsymbol{e}_4 \\ \dot{\boldsymbol{e}}_4 = -(c_1 + c_2)\boldsymbol{e}_4 - (c_1 c_2 + 1)\boldsymbol{e}_3 - \boldsymbol{M}_{11}^{-1} \boldsymbol{J}_{p\theta}^{\mathrm{T}} (\varepsilon \boldsymbol{\tau}_1 + \varepsilon^2 \boldsymbol{\tau}_2) - \varepsilon^2 \boldsymbol{J}_{12} (\boldsymbol{J}_{22})_0^{-1} \ddot{\boldsymbol{h}}_{10} \\ \quad - \varepsilon^2 \left(\boldsymbol{J}_{p\theta}^{-1} \boldsymbol{\phi}_l \ddot{\boldsymbol{h}}_{10} + \dot{\overline{\boldsymbol{J}_{p\theta}^{-1}}} \boldsymbol{\phi}_l \dot{\boldsymbol{h}}_{10} \right)/l_1 + \varepsilon^2 \boldsymbol{M}_{11}^{-1} \left((\boldsymbol{f}_1)_{20} \boldsymbol{h}_{10} + (\boldsymbol{f}_1)_{21} \dot{\boldsymbol{h}}_{10} \right)/2 - \varepsilon^2 (c_1 c_2 + 1) \boldsymbol{J}_{p\theta}^{-1} \boldsymbol{\phi}_l \boldsymbol{h}_{10}/l_1 \\ \quad - \varepsilon^2 \boldsymbol{J}_{12} (\boldsymbol{J}_{22})_0^{-1} (\boldsymbol{J}_{22})_2 \left((\boldsymbol{f}_2)_0 + \boldsymbol{h}_{10} \right)/2 - \varepsilon^2 (c_1 + c_2) \boldsymbol{J}_{p\theta}^{-1} \boldsymbol{\phi}_l \dot{\boldsymbol{h}}_{10}/l_1 - \varepsilon^2 \boldsymbol{J}_{12} (\boldsymbol{f}_2)_{21} \dot{\boldsymbol{h}}_{10}/2 \end{cases} \tag{26}$$

According to Eq. (26), define the Lyapunov function,

http://dx.doi.org/10.5772/intechopen.80375

$$\boldsymbol{V}_3 = 1/2\boldsymbol{e}_3^{\mathrm{T}}\left(c_1c_2+1\right)\boldsymbol{e}_3 + 1/2\boldsymbol{e}_4^{\mathrm{T}}\boldsymbol{e}_4. \tag{27}$$

Derivative of Eq. (27) with respect to time can be obtained as,

$$\begin{aligned}\dot{\boldsymbol{V}}_3 &= 1/2\boldsymbol{e}_3^{\mathrm{T}}\left(c_1c_2+1\right)\dot{\boldsymbol{e}}_3 + 1/2\boldsymbol{e}_4^{T}\dot{\boldsymbol{e}}_4 = \\ &-1/2\boldsymbol{e}_4^{\mathrm{T}}\left(c_1+c_2\right)\boldsymbol{e}_4 + 1/2\boldsymbol{e}_4^{\mathrm{T}}\left(-\boldsymbol{M}_{11}^{-1}\boldsymbol{J}_{p\theta}^{\mathrm{T}}\left(\varepsilon\boldsymbol{\tau}_1+\varepsilon^2\boldsymbol{\tau}_2\right)-\varepsilon^2\left(\boldsymbol{J}_{p\theta}^{-1}\phi_l\ddot{\boldsymbol{h}}_{10}+\dot{\overline{\boldsymbol{J}_{p\theta}^{-1}}}\phi_l\dot{\boldsymbol{h}}_{10}\right)/l_1+\right. \\ &\left.\varepsilon^2\boldsymbol{M}_{11}^{-1}\left(\left(\boldsymbol{f}_1\right)_{20}\boldsymbol{h}_{10}+\left(\boldsymbol{f}_1\right)_{21}\dot{\boldsymbol{h}}_{10}\right)/2-\varepsilon^2\boldsymbol{J}_{12}\left(\boldsymbol{J}_{22}\right)_0^{-1}\left(\boldsymbol{J}_{22}\right)_2\left(\left(\boldsymbol{f}_2\right)_0+\boldsymbol{h}_{10}\right)/2-\varepsilon^2\left(c_1+c_2\right)\boldsymbol{J}_{p\theta}^{-1}\phi_l\dot{\boldsymbol{h}}_{10}/l_1-\right. \\ &\left.\varepsilon^2\boldsymbol{J}_{12}\left(\boldsymbol{J}_{22}\right)_0^{-1}\ddot{\boldsymbol{h}}_{10}-\varepsilon^2\left(c_1c_2+1\right)\boldsymbol{J}_{p\theta}^{-1}\phi_l\boldsymbol{h}_{10}/l_1-\varepsilon^2\boldsymbol{J}_{12}\left(\boldsymbol{f}_2\right)_{21}\dot{\boldsymbol{h}}_{10}/2\right).\end{aligned} \tag{28}$$

Let the coefficient of ε and ε^2 be zero, and the corrective torque is,

$$\begin{aligned}&\boldsymbol{\tau}_1 = 0,\\ &\boldsymbol{\tau}_2 = -\left(\boldsymbol{J}_{p\theta}^{\mathrm{T}}\right)^{-1}\boldsymbol{M}_{11}\left((c_1+c_2)\left(\boldsymbol{J}_{p\theta}^{-1}\phi_l\dot{\boldsymbol{h}}_{10}\right)/l_1+(c_1c_2+1)\boldsymbol{J}_{p\theta}^{-1}\phi_l\boldsymbol{h}_{10}/l_1-\boldsymbol{M}_{11}^{-1}\left(\left(\boldsymbol{f}_1\right)_{20}\boldsymbol{h}_{10}+\left(\boldsymbol{f}_1\right)_{21}\dot{\boldsymbol{h}}_{10}\right)/2\right.\\ &\left.+\boldsymbol{J}_{12}(\boldsymbol{J}_{22})_0^{-1}(\boldsymbol{J}_{22})_2(\boldsymbol{f}_2+\boldsymbol{h}_{10})/2+\boldsymbol{J}_{12}(\boldsymbol{J}_{22})_0^{-1}\ddot{\boldsymbol{h}}_{10}+\left(\boldsymbol{J}_{p\theta}^{-1}\phi_l\ddot{\boldsymbol{h}}_{10}+\dot{\overline{\boldsymbol{J}_{p\theta}^{-1}}}\phi_l\dot{\boldsymbol{h}}_{10}\right)/l_1+\boldsymbol{J}_{12}\left(\boldsymbol{f}_2\right)_{21}\dot{\boldsymbol{h}}_{10}/2\right)\end{aligned} \tag{29}$$

At this time, $\dot{\boldsymbol{V}} = -\boldsymbol{e}_4^{\mathrm{T}}(c_1+c_2)\boldsymbol{e}_4 \le 0$ is valid, and the system is stable, which means the elastic displacement compensation for the end-effector's pose is realized by designing the corrective torque.

5. Sliding mode variable structure-based fast subsystem control

Define a new time scale $t_f = t/\varepsilon$, and the fast subsystem differential Eq. (12) can be expressed as,

$$\begin{cases}\dfrac{\mathrm{d}\boldsymbol{X}_{f1}}{\mathrm{d}t_f} = \boldsymbol{X}_{f2},\\ \dfrac{\mathrm{d}\boldsymbol{X}_{f2}}{\mathrm{d}t_f} = \boldsymbol{J}_{12}^{\mathrm{T}}\boldsymbol{J}_{p\theta}^{\mathrm{T}}\boldsymbol{\tau}_f-(\boldsymbol{J}_{22})_0\boldsymbol{X}_{f1}-\varepsilon^2\left((\boldsymbol{J}_{22})_2+\boldsymbol{J}_{12}^{\mathrm{T}}\left(\boldsymbol{f}_1\right)_{20}\right)\boldsymbol{X}_{f1}/2-\varepsilon\boldsymbol{J}_{12}^{\mathrm{T}}\left(\boldsymbol{f}_1\right)_{21}\boldsymbol{X}_{f2}/2\end{cases} \tag{30}$$

The latter two terms of the second equation contain small parameter ε, and the control amount is small compared to other terms, which can be regarded as the disturbance, so the disturbance term can be expressed as,

$$\boldsymbol{\Delta}_1 = \varepsilon^2\left((\boldsymbol{J}_{22})_2+\boldsymbol{J}_{12}^{\mathrm{T}}\left(\boldsymbol{f}_1\right)_{20}\right)\boldsymbol{X}_{f1}/2-\varepsilon\left(\boldsymbol{J}_{12}^{\mathrm{T}}\left(\boldsymbol{f}_1\right)_{21}+(\boldsymbol{J}_{22})_0\left(\boldsymbol{f}_2\right)_{21}\right)\boldsymbol{X}_{f2}/2. \tag{31}$$

Due to the existence of the disturbance term, the fast subsystem adopts sliding mode variable structure control, and the sliding mode surface is selected as,

$$\boldsymbol{S}(t) = \boldsymbol{K}_f\boldsymbol{X}_{f1}+\boldsymbol{X}_{f2}. \tag{32}$$

where $\boldsymbol{K}_1$ is a positive number, the derivation of the upper sliding surface can be obtained,

$$\dot{\boldsymbol{S}}(t) = \boldsymbol{K}_f \boldsymbol{X} + \boldsymbol{J}_{12}^{\mathrm{T}} \boldsymbol{J}_{p\theta}^{\mathrm{T}} \boldsymbol{\tau}_f - (\boldsymbol{J}_{22})_0 \boldsymbol{X}_{f1} - \boldsymbol{\Delta}_1. \tag{33}$$

According to the sliding surface, the Lyapunov function is defined as,

$$\boldsymbol{V}_4 = 1/2 \boldsymbol{S}^{\mathrm{T}} \boldsymbol{S}. \tag{34}$$

Derivative of the above equation with respect to time can be obtained as,

$$\dot{\boldsymbol{V}}_4 = \boldsymbol{S}^{\mathrm{T}} \dot{\boldsymbol{S}} = \boldsymbol{S}^{\mathrm{T}} \left(\boldsymbol{K}_f \boldsymbol{X}_{f2} + \boldsymbol{J}_{12}^{\mathrm{T}} \boldsymbol{J}_{p\theta}^{\mathrm{T}} \boldsymbol{\tau}_f - (\boldsymbol{J}_{22})_0 \boldsymbol{X}_{f1} - \boldsymbol{\Delta}_1 \right) \tag{35}$$

According to Eq. (35), the fast subsystem control law designed as,

$$\boldsymbol{\tau}_f = \left(\boldsymbol{J}_{12}^{\mathrm{T}} \boldsymbol{J}_{p\theta}^{\mathrm{T}} \right)^{-1} \left(-\boldsymbol{K}_f \boldsymbol{X}_{f2} + (\boldsymbol{J}_{22})_0 \boldsymbol{X}_{f1} - \boldsymbol{K}_f \boldsymbol{S} + \boldsymbol{\Delta}_1 \operatorname{sgn}(\boldsymbol{S}) \right). \tag{36}$$

where $\operatorname{sgn}(\cdot)$ is the sign function, substituting Eq. (36) into (35) can be obtained,

$$\dot{\boldsymbol{V}}_4 = \boldsymbol{S}^{\mathrm{T}} \left(\boldsymbol{K}_f \boldsymbol{X} + \boldsymbol{J}_{12}^{\mathrm{T}} \boldsymbol{J}_{p\theta}^{\mathrm{T}} \boldsymbol{\tau}_f - (\boldsymbol{J}_{22})_0 \boldsymbol{X}_{f1} - \boldsymbol{\Delta}_1 \right) = -\boldsymbol{\Delta}_1 |\boldsymbol{S}| - \boldsymbol{\Delta}_1 \boldsymbol{S} - \boldsymbol{S}^{\mathrm{T}} \boldsymbol{K}_f \boldsymbol{S} \leq -\boldsymbol{S}^{\mathrm{T}} \boldsymbol{K}_f \boldsymbol{S} \leq 0 \tag{37}$$

Therefore, according to the Lyapunov stability principle, the fast subsystem is convergent with torque of (36). The symbolic function will cause jitter to the system. To reduce the generation of jitter, the saturation function $sat(\cdot)$ is substituted for the symbol function. The saturation function can be defined as [20],

$$sat(s_1) = \begin{cases} 1, & s_1 > \Delta_2; \\ s_1/\Delta_2, & |s_1| \leq \Delta_2; \\ -1, & s_1 < -\Delta_2. \end{cases} \tag{38}$$

where Δ_2 is the buffer layer.

6. The high-gain observer for the curvature change rate

The curvature can be obtained by strain gage measurement of the stress of the links, and the change rate of curvature is directly related to the rate of change of stress, and generally cannot be directly measured. In order to avoid direct measurement of the change rate of curvature, this chapter will design a high-gain observer to observe the curvature change rate by measuring the curvature. It can be known from Eq. (11) that the fast subsystem variable $\boldsymbol{X}_{f1}$ corresponds to the curvature, which can be directly converted by measuring the stress. $\boldsymbol{X}_{f2}$ corresponds to observed curvature change rate. According to the literature [21, 22] and the formula (4), the observer can be expressed as,

$$\begin{cases} \varepsilon\dot{\hat{\boldsymbol{X}}}_{f1} = \hat{\boldsymbol{X}}_{f2} + \dfrac{1}{\varepsilon_1}\boldsymbol{H}_p\left(\boldsymbol{X}_{f1} - \hat{\boldsymbol{X}}_{f1}\right), \\ \varepsilon\dot{\hat{\boldsymbol{X}}}_{f2} = \dfrac{1}{\varepsilon_1^2}\boldsymbol{H}_v\left(\boldsymbol{X}_{f1} - \hat{\boldsymbol{X}}_{f1}\right). \end{cases} \tag{39}$$

where $\hat{\boldsymbol{X}}_{f1}$ and $\hat{\boldsymbol{X}}_{f2}$ represent the estimated values of $\boldsymbol{X}_{f1}$ and $\boldsymbol{X}_{f2}$, respectively, ε_1 is the minimum positive number, $\boldsymbol{H}_p$ and $\boldsymbol{H}_v$ are the constant matrix, the observer tracking error is defined as,

$$\begin{cases} \tilde{\boldsymbol{X}}_{f1} = \hat{\boldsymbol{X}}_{f1} - \boldsymbol{X}_{f1}, \\ \tilde{\boldsymbol{X}}_{f2} = \hat{\boldsymbol{X}}_{f2} - \boldsymbol{X}_{f2}. \end{cases} \tag{40}$$

To prove the stability of the system, new variables of error are defined as,

$$\begin{cases} \tilde{\boldsymbol{Z}}_{f1} = \tilde{\boldsymbol{X}}_{f1}, \\ \tilde{\boldsymbol{Z}}_{f2} = \varepsilon_1\tilde{\boldsymbol{X}}_{f2}. \end{cases} \tag{41}$$

Substitute the above equation into (39), the state observer can be expressed as,

$$\begin{cases} \varepsilon\varepsilon_1\dot{\tilde{\boldsymbol{Z}}}_{f1} = \tilde{\boldsymbol{Z}}_{f2} - \boldsymbol{H}_p\tilde{\boldsymbol{Z}}_{f1}, \\ \varepsilon\varepsilon_1\dot{\tilde{\boldsymbol{Z}}}_{f2} = -\boldsymbol{H}_v\tilde{\boldsymbol{Z}}_{f1} + \varepsilon\varepsilon_1^2\left(\boldsymbol{J}_{12}^{\mathrm{T}}\boldsymbol{J}_{p\theta}^{\mathrm{T}}\boldsymbol{\tau}_f - (\boldsymbol{J}_{22})_0\boldsymbol{X}_{f1} - \boldsymbol{\Delta}_1\right) \end{cases} \tag{42}$$

The Eq. (42) can be rewritten as,

$$\varepsilon\varepsilon_1\dot{\tilde{\boldsymbol{Z}}}_f = \boldsymbol{A}_0\tilde{\boldsymbol{Z}}_f + \varepsilon\varepsilon_1^2\boldsymbol{B}_0\left(\boldsymbol{J}_{12}^{\mathrm{T}}\boldsymbol{J}_{p\theta}^{\mathrm{T}}\boldsymbol{\tau}_f - (\boldsymbol{J}_{22})_0\boldsymbol{X}_{f1} - \boldsymbol{\Delta}_1\right). \tag{43}$$

where $\boldsymbol{A}_0 = \begin{bmatrix} -\boldsymbol{H}_p & \boldsymbol{I}_{3\times3} \\ -\boldsymbol{H}_v & \boldsymbol{0}_{3\times3} \end{bmatrix}$ and $\boldsymbol{B}_0 = \begin{bmatrix} \boldsymbol{0}_{3\times3} \\ \boldsymbol{I}_{3\times3} \end{bmatrix}$. All eigenvalues of $\boldsymbol{A}_0$ can be guaranteed negative by selecting $\boldsymbol{H}_p$ and $\boldsymbol{H}_v$, which means that $\boldsymbol{A}_0$ is the Hurwitz matrix. Define a new Lyapunov function as,

$$\boldsymbol{V}_6 = \tilde{\boldsymbol{Z}}_f^{\mathrm{T}}\boldsymbol{P}_1\tilde{\boldsymbol{Z}}_f. \tag{44}$$

where $\boldsymbol{P}_1$ is the positive definite symmetry matrix, the derivation is expressed as,

$$\dot{\boldsymbol{V}}_6 = \frac{1}{\varepsilon\varepsilon_1}\left(\tilde{\boldsymbol{Z}}_f^{\mathrm{T}}\left(\boldsymbol{A}_0^{\mathrm{T}}\boldsymbol{P}_1 + \boldsymbol{P}_1\boldsymbol{A}_0\right)\tilde{\boldsymbol{Z}}_f + 2\varepsilon\varepsilon_1^2\cdot\left(\boldsymbol{J}_{12}^{\mathrm{T}}\boldsymbol{J}_{p\theta}^{\mathrm{T}}\boldsymbol{\tau}_f - (\boldsymbol{J}_{22})_0\boldsymbol{X}_{f1} - \boldsymbol{\Delta}_1\right)^{\mathrm{T}}\boldsymbol{B}_0^{\mathrm{T}}\boldsymbol{P}_1\tilde{\boldsymbol{Z}}_f\right). \tag{45}$$

Since $\boldsymbol{A}_0$ is a Hurwitz matrix, there is a positive definite matrix $\boldsymbol{P}_1$, which makes,

$$\boldsymbol{A}_0^{\mathrm{T}}\boldsymbol{P}_1+\boldsymbol{P}_1\boldsymbol{A}_0=-\boldsymbol{I}_{3\times3}. \tag{46}$$

$\dot{\boldsymbol{V}}_6$ can be rewritten as,

$$\dot{\boldsymbol{V}}_6\le-\frac{1}{\varepsilon\varepsilon_1}\left\|\tilde{\boldsymbol{Z}}_f\right\|^2+2\varepsilon_1\left\|\left(\boldsymbol{J}_{12}^{\mathrm{T}}\boldsymbol{J}_{p\theta}^{\mathrm{T}}\boldsymbol{\tau}_f-(\boldsymbol{J}_{22})_0\boldsymbol{X}_{f1}-\boldsymbol{\Delta}_1\right)^{\mathrm{T}}\boldsymbol{B}_0^{\mathrm{T}}\boldsymbol{P}_1\right\|\left\|\tilde{\boldsymbol{Z}}_f\right\|. \tag{47}$$

According to Eq. (47), when ε_1^2 satisfied the following relationship, $\dot{\boldsymbol{V}}_6\le0$ is established, which means the high-gain observer gradually converges,

$$\varepsilon_1^2\le\frac{2\left\|\left(\boldsymbol{J}_{12}^{\mathrm{T}}\boldsymbol{J}_{p\theta}^{\mathrm{T}}\boldsymbol{\tau}_f-(\boldsymbol{J}_{22})_0\boldsymbol{X}_{f1}-\boldsymbol{\Delta}_1\right)^{\mathrm{T}}\boldsymbol{B}_0^{\mathrm{T}}\boldsymbol{P}_1\right\|}{\varepsilon\left\|\tilde{\boldsymbol{Z}}_f\right\|}. \tag{48}$$

Therefore, according to Eq. (48), the upper bound of the small parameter can be obtained, and the fast subsystem torque can be expressed as,

$$\boldsymbol{\tau}_f=\left(\boldsymbol{J}_{12}^{\mathrm{T}}\boldsymbol{J}_{p\theta}^{\mathrm{T}}\right)^{-1}\left(-\boldsymbol{K}_f\hat{\boldsymbol{X}}_{f2}+(\boldsymbol{J}_{22})_0\hat{\boldsymbol{X}}_{f1}-\ \boldsymbol{K}_f\hat{\boldsymbol{S}}+\boldsymbol{\Delta}_1sat\left(\hat{\boldsymbol{S}}\right)\right). \tag{49}$$

where $\hat{\boldsymbol{S}}=\boldsymbol{K}_f\hat{\boldsymbol{X}}_{f1}+\hat{\boldsymbol{X}}_{f2}$. According to Eq. (12) and (42), the error equation of the fast subsystem can be expressed as,

$$\varepsilon\dot{\boldsymbol{\xi}}=\boldsymbol{A}_\xi\boldsymbol{\xi}+\boldsymbol{h}_\xi \tag{50}$$

where

$$\boldsymbol{\xi}=\left[\boldsymbol{X}_f\ \tilde{\boldsymbol{Z}}_f\right]^{\mathrm{T}},\ \boldsymbol{X}_f=\left[\boldsymbol{X}_{f1}\ \boldsymbol{X}_{f2}\right]^{\mathrm{T}},\ \boldsymbol{A}_\xi=\begin{bmatrix}\boldsymbol{A}_{\xi11}&\boldsymbol{A}_{\xi12}\\0&\boldsymbol{A}_0/\varepsilon_1\end{bmatrix},\boldsymbol{A}_{\xi11}=\begin{bmatrix}\boldsymbol{0}_{3\times3}&\boldsymbol{I}_{3\times3}\\-\boldsymbol{K}_f^2&-2\boldsymbol{K}_f\end{bmatrix},$$

$$\boldsymbol{A}_{\xi12}=\begin{bmatrix}\boldsymbol{0}_{3\times3}&\boldsymbol{0}_{3\times3}\\(\boldsymbol{J}_{22})_0-\boldsymbol{K}_f^2&-2\boldsymbol{K}_f\end{bmatrix},\ \boldsymbol{h}_\xi=\begin{bmatrix}\boldsymbol{\Delta}_1sat\left(\hat{\boldsymbol{S}}\right)-\boldsymbol{\Delta}_1\\\varepsilon\varepsilon_1\boldsymbol{B}_0\left(\boldsymbol{J}_{12}^{\mathrm{T}}\boldsymbol{J}_{p\theta}^{\mathrm{T}}\boldsymbol{\tau}_f-(\boldsymbol{J}_{22})_0\boldsymbol{X}_{f1}-\boldsymbol{\Delta}_1\right)\end{bmatrix}.$$

According to Eq. (50), the Lyapunov function can be defined as:

$$\boldsymbol{V}_5=\varepsilon\boldsymbol{\xi}^T\boldsymbol{P}_\xi\boldsymbol{\xi} \tag{51}$$

where $\boldsymbol{P}_\xi$ is the symmetric positive definite matrix, Eq. (51) is derived as,

$$\boldsymbol{V}_5=\varepsilon\boldsymbol{\xi}^{\mathrm{T}}\left(\boldsymbol{A}_\xi^{\mathrm{T}}\boldsymbol{P}_\xi+\boldsymbol{P}_\xi^{\mathrm{T}}\boldsymbol{A}_\xi\right)\boldsymbol{\xi}+2\boldsymbol{h}_\xi^{\mathrm{T}}\boldsymbol{P}_\xi\boldsymbol{\xi}+\varepsilon\boldsymbol{\xi}^{\mathrm{T}}\dot{\boldsymbol{P}}_\xi\boldsymbol{\xi}. \tag{52}$$

Since $\boldsymbol{A}_{\xi11}$ and $\boldsymbol{A}_0$ are Hurwitz matrix, for a given symmetric positive definite matrix S_ξ, there is a symmetric positive definite matrix $\boldsymbol{P}_\xi$ that satisfies the following conditions,

$$\boldsymbol{A}_\xi^{\mathrm{T}}\boldsymbol{P}_\xi+\boldsymbol{P}_\xi^{\mathrm{T}}\boldsymbol{A}_\xi=-\boldsymbol{S}_\xi. \tag{53}$$

According to the Rayleigh-Ritz inequality,

$$-\boldsymbol{\xi}^{\mathrm{T}}\boldsymbol{S}_{\xi}\boldsymbol{\xi} \leq -\lambda_{\min}(\boldsymbol{S}_{\xi})\|\boldsymbol{\xi}\|^{2}, \tag{54}$$

$$\left\|\boldsymbol{h}_{\xi}^{\mathrm{T}}\boldsymbol{P}_{\xi}\boldsymbol{\xi}\right\| \leq (\chi_0 + \chi_1\varepsilon_1)\|\boldsymbol{\xi}\|, \left\|\dot{\boldsymbol{P}}_{\xi}\right\| \leq \chi_2. \tag{55}$$

where $\lambda_{\min}(\cdot)$ represents the minimum eigenvalues of the corresponding matrix. χ_0, χ_1, and χ_2 are positive real numbers. According to Eqs. (53) through (55), Eq. (52) can be expressed as,

$$\dot{\boldsymbol{V}}_5 \leq -\lambda_{\min}\left(\boldsymbol{S}_{\xi}\right)\|\boldsymbol{\xi}\|^{2} + \varepsilon\chi_2\|\boldsymbol{\xi}\|^{2} + 2(\chi_0 + \chi_1\varepsilon_1)\|\boldsymbol{\xi}\|. \tag{56}$$

According to Eq. (56), when $\dot{\boldsymbol{V}}_5 \leq 0$, the small parameters in the high-gain observer satisfied $0 \leq \varepsilon_1 \leq \varepsilon_{1\max}$, the fast subsystem based on the high-gain observer is stable, and the upper bound of the small parameter satisfies the following requirements,

$$\varepsilon_{1\max} \leq (\lambda_{\min}(\boldsymbol{S}_{\xi})\|\boldsymbol{\xi}\| - \varepsilon\chi_2\|\boldsymbol{\xi}\| - 2\chi_0)/\chi_1. \tag{57}$$

7. Stability proof of the system

The abovementioned integral manifold is used to reduce the rigid-flexible coupling system of high-speed PM, and the complex high-order system is decomposed into a slow subsystem describing the rigid body motion and a fast subsystem of elastic deformation, and the backstepping control and sliding mode variable structure control are adopted for two subsystems, respectively, and designed a high-gain observer to solve the problem that the elastic displacement change rate is difficult to measure, and proved the stability of each subsystem. However, the stability of each subsystem does not guarantee the stability of the overall system. Therefore, it is necessary to synthesize the subsystems to prove the stability of the overall system. Substituting Eqs. (9), (20), and (29) into kinetic Eq. (3), the systematic error equation can obtained,

$$\dot{\boldsymbol{e}}_s = \boldsymbol{A}_s\boldsymbol{e}_s + \boldsymbol{h}_s, \varepsilon\dot{\boldsymbol{\xi}} = \boldsymbol{A}_{\xi}\boldsymbol{\xi} + \boldsymbol{h}_{\xi}. \tag{58}$$

where

$$\boldsymbol{e}_s = \left[\boldsymbol{X}_1 - \boldsymbol{X}_d \;\; \dot{\boldsymbol{X}}_1 - \dot{\boldsymbol{X}}_d\right]^{\mathrm{T}}, \boldsymbol{h}_s = \begin{bmatrix} 0 \\ \boldsymbol{h}_{s1} \end{bmatrix}, \boldsymbol{A}_s = \begin{bmatrix} \boldsymbol{0}_{3\times3} & \boldsymbol{I}_{3\times3} \\ -(c_1c_2+1)\boldsymbol{I}_{3\times3} & -(c_1+c_2)\boldsymbol{I}_{3\times3} \end{bmatrix},$$

$$\boldsymbol{h}_{s1} = \boldsymbol{J}_{11}\boldsymbol{J}_{p\theta}^{\mathrm{T}}\boldsymbol{\tau}_f - \boldsymbol{J}_{12}\boldsymbol{X}_{f1} - \varepsilon^2\boldsymbol{J}_{11}\boldsymbol{M}_{11}\Big((c_1+c_2)\boldsymbol{J}_{p\theta}^{-1}\phi_l\dot{\boldsymbol{h}}_{10}/l_1 + (c_1c_2+1)\boldsymbol{J}_{p\theta}^{-1}\phi_l\boldsymbol{h}_{10}/l_1$$
$$+\left(\boldsymbol{J}_{p\theta}^{-1}\phi_l\ddot{\boldsymbol{h}}_{10} + \dot{\overline{\boldsymbol{J}_{p\theta}^{-1}}}\phi_l\dot{\boldsymbol{h}}_{10}\right)/l_1\Big).$$

According to the error equation, define the Lyapunov function that contains the overall system as,

$$\boldsymbol{V}_6 = \boldsymbol{e}_s^{\mathrm{T}}\boldsymbol{P}_s\boldsymbol{e}_s + \varepsilon\boldsymbol{\xi}^{\mathrm{T}}\boldsymbol{P}_{\xi}\boldsymbol{\xi}. \tag{59}$$

where $\boldsymbol{P}_s$ and $\boldsymbol{P}_\xi$ are the symmetric positive definite matrix, the derivative of Eq. (59) can be obtained,

$$\dot{\boldsymbol{V}}_6 = \boldsymbol{e}_s^{\mathrm{T}}\left(\boldsymbol{A}_s^{\mathrm{T}}P_s + \boldsymbol{P}_s^{\mathrm{T}}\boldsymbol{A}_s\right)\boldsymbol{e}_s + \boldsymbol{\xi}^{\mathrm{T}}\left(\boldsymbol{A}_\xi^{\mathrm{T}}\boldsymbol{P}_\xi + \boldsymbol{P}_\xi^{\mathrm{T}}\boldsymbol{A}_\xi\right)\boldsymbol{\xi} + 2\boldsymbol{h}_s^{\mathrm{T}}\boldsymbol{P}_s\boldsymbol{e}_s + 2\boldsymbol{h}_\xi^{\mathrm{T}}\boldsymbol{P}_\xi\boldsymbol{\xi} + \varepsilon\boldsymbol{\xi}^{\mathrm{T}}\dot{\boldsymbol{P}}_\xi\boldsymbol{\xi}. \tag{60}$$

Since $\boldsymbol{A}_s$ is a Hurwitz matrix, for a given symmetric positive definite matrix $\boldsymbol{S}_s$, there is a symmetric positive definite matrix $\boldsymbol{P}_s$ that satisfies the following conditions,

$$\boldsymbol{A}_s^{\mathrm{T}}\boldsymbol{P}_s + \boldsymbol{P}_s^{\mathrm{T}}\boldsymbol{A}_s = -\boldsymbol{S}_s. \tag{61}$$

According to Eqs. (53) and (61), $\dot{\boldsymbol{V}}_6$ can be rewritten as,

$$\dot{\boldsymbol{V}}_6 = -\boldsymbol{e}_s^{\mathrm{T}}\boldsymbol{S}_s\boldsymbol{e}_s - \boldsymbol{\xi}^{\mathrm{T}}\boldsymbol{S}_\xi\boldsymbol{\xi} + 2\boldsymbol{h}_s^{\mathrm{T}}P_s\boldsymbol{e}_s + 2\boldsymbol{h}_\xi^{\mathrm{T}}P_\xi\boldsymbol{\xi} + \varepsilon\boldsymbol{\xi}^{\mathrm{T}}\dot{P}_\xi\boldsymbol{\xi} \tag{62}$$

According to the Rayleigh-Ritz inequality, we can obtain,

$$-\boldsymbol{e}_s^{\mathrm{T}}\boldsymbol{S}_s\boldsymbol{e}_s \le -\lambda_{\min}(\boldsymbol{S}_s)\|\boldsymbol{e}_s\|^2, \tag{63}$$

$$-\boldsymbol{\xi}^{\mathrm{T}}\boldsymbol{S}_\xi\boldsymbol{\xi} \le -\lambda_{\min}(\boldsymbol{S}_\xi)\|\boldsymbol{\xi}\|^2, \tag{64}$$

$$\left\|\boldsymbol{h}_s^{\mathrm{T}}\boldsymbol{P}_s\boldsymbol{e}_s\right\| \le \left(\chi_3 + \chi_4\varepsilon + \chi_5\varepsilon^2\right)\|\boldsymbol{e}_s\|\|\boldsymbol{\xi}\|, \tag{65}$$

$$\left\|\boldsymbol{h}_\xi^{\mathrm{T}}\boldsymbol{P}_\xi\boldsymbol{\xi}\right\| \le \left(\chi_6 + \chi_7\varepsilon + \chi_8\varepsilon^2\right)\|\boldsymbol{\xi}\|^2. \tag{66}$$

where $\chi_i(i = 0, 1, \ldots 6)$ is positive. According to the inequality relationship shown by Eqs. (63) to (66), $\dot{\boldsymbol{V}}_6$ satisfied the following relationship,

$$\dot{\boldsymbol{V}}_6 \le -\left[\,\|\boldsymbol{e}_s\| \quad \|\boldsymbol{\xi}\|\,\right]\cdot\begin{bmatrix}\lambda_{\min}(S_s) & -\left(\chi_3 + \chi_4\varepsilon + \chi_5\varepsilon^2\right) \\ -\left(\chi_3 + \chi_4\varepsilon + \chi_5\varepsilon^2\right) & \lambda_{\min}(S_\xi) - 2\left(\chi_6 + \chi_7\varepsilon + \chi_8\varepsilon^2\right) - \chi_2\varepsilon\end{bmatrix}\begin{bmatrix}\|\boldsymbol{e}_s\| \\ \|\boldsymbol{\xi}\|\end{bmatrix}. \tag{67}$$

The condition that the closed-loop system is asymptotically stable is $\dot{\boldsymbol{V}}_6 \le 0$, from the above equation, the condition of $\dot{\boldsymbol{V}}_6 \le 0$ is that the coefficient matrix is positive, that is,

$$\lambda_{\min}(S_s)\left(\lambda_{\min}(S_\xi) - 2\left(\chi_6 + \chi_7\varepsilon + \chi_8\varepsilon^2\right) - \chi_2\varepsilon\right) - \left(\chi_3 + \chi_4\varepsilon + \chi_5\varepsilon^2\right)^2 \ge 0. \tag{68}$$

Ignoring the influence of high-order terms of $O(\varepsilon^2)$, when the maximum value of the small parameter ε satisfied,

$$\varepsilon_{\max} = \frac{-\lambda_b + \sqrt{\lambda_b^2 + 4\lambda_a\lambda_c}}{2\lambda_a}. \tag{69}$$

$\dot{\boldsymbol{V}}_6 \le 0$ is valid, where

http://dx.doi.org/10.5772/intechopen.80375

$$\begin{cases} \lambda_a = \lambda_{\min}(S_s)\chi_8 + \chi_4^2 + 2\chi_3\chi_5, \\ \lambda_b = -2\lambda_{\min}(S_s)\chi_7 - \lambda_{\min}(S_s)\chi_2 - 2\chi_3\chi_4, \\ \lambda_c = \lambda_{\min}(S_s)\lambda_{\min}(S_\xi) - 2\lambda_{\min}(S_s)\chi_6 - \chi_3^2. \end{cases} \tag{70}$$

According to Eq. (67), when the value of ε satisfied $0 < \varepsilon \le \varepsilon_{\max}$, the overall system is stable.

8. Algorithm simulations

When the Taylor expanding order $p = 0$ is valid, the integral manifold (IM) is equivalent to the singular perturbation (SP). In order to verify the composite control proposed in this chapter, this section compares it with the singular perturbation control and the backstepping (BS) control considering only the rigid-body dynamic model. The above algorithm simulation will be carried out under the SIMULINK module of the MATLAB software, and the ode15s integral will be selected. According to formula (29), in the composite control algorithm based on the integral manifold and observer, the desired trajectory of the end-effector of the moving platform needs to satisfy the fourth derivative continuous, and at the same time to reduce the impact to the system at the beginning and end point of the desired trajectory. The nine-order polynomial shown in Eq. (71) is used to ensure that the velocity, acceleration, and the third and fourth derivatives at the start and end points are zero.

$$\begin{cases} p_x = A_0\left(125t^5/t_d^5 - 420t^6/t_d^6 + 540t^7/t_d^7 - 315t^8/t_d^8 + 70t^9/t_d^9\right) + p_{x0}, \\ p_y = p_{y0}, \\ \phi = 0. \end{cases} \tag{71}$$

where the running time t_{d} is 0.06 s, the starting position $p_{x0} = 187.5$, $p_{y0} = 187.5/\sqrt{3}$, and the amplitude $A_0 = 30$ of the desired trajectory. Take $\varepsilon^2 = 1/k_s$, $\boldsymbol{\Delta}_1 = 1 \times 10^{-3}$, $c_1 = c_2 = 50$, $\Delta_2 = 0.05$, $\boldsymbol{H}_p = \mathbf{diag}([40, 40, 40])$, $\boldsymbol{H}_v = \mathbf{diag}([400, 400, 400])$, $\boldsymbol{K}_f = \mathbf{diag}([60, 60, 60])$. According to Eq. (57), take $\varepsilon_1 = 0.001$. The parameters added and modified in [17] are as follows: the height and thickness of the links are 30 and 5 mm, respectively, the reduction ratio is 20, and the moment of inertia between the motor and the reducer is 284.1 $kg \cdot mm^2$.

To describe the control performance of the end-effector, an average error is introduced, and is defined as,

$$\begin{cases} t_{\mathrm{M}} = \sqrt{\dfrac{1}{t_d}\displaystyle\int_0^{t_d}\left(\boldsymbol{C}_R(1)^2 + \boldsymbol{C}_R(2)^2\right)\mathrm{dt}} \\ r_{\mathrm{M}} = \sqrt{\dfrac{1}{t_d}\displaystyle\int_0^{t_d}\boldsymbol{C}_R(3)^2\mathrm{dt}} \end{cases} \tag{72}$$

where C_R represents the performance index of the three directions of the moving platform, t_{rM} and r_M are the average error of the translation direction and the rotation direction.

According to Eq. (24), the elastic displacement f_3 of the moving platform can be calculated. v_i and v_m represent the maximum elastic displacement and the average elastic displacement in all directions of the moving platform during operation, v_{end} indicates the elastic displacement at the end point (residual vibration). For the same expected input, the magnitude of the elastic displacement of the moving platform can reflect the vibration suppression effect of the three control algorithms. The elastic displacements in all directions are shown in **Figures 4** and **5**, which shows that the maximum elastic displacement amplitude in all directions is reduced by more than 28% compared with the backstepping control, and the composite control is reduced by 4.75, 33.42, and 33.52% compared with the singular perturbation. The average elastic displacement for the translational direction decreases from 1.579 and 1.112 mm for backstepping control and singular perturbation to 0.970 mm for composite control. For the rotational direction, 0.0014 and 9.863×10^{-4} rad from backstepping control and singular perturbation drops to 6.872×10^{-4} rad of the composite control. Compared with the above algorithm, the elastic displacement of the composite control decreases by more than 14% in both directions. Compared with the backstepping control, when the composite control and the singular perturbation algorithm are used, the residual vibration is greatly reduced, and both algorithms are close to zero.

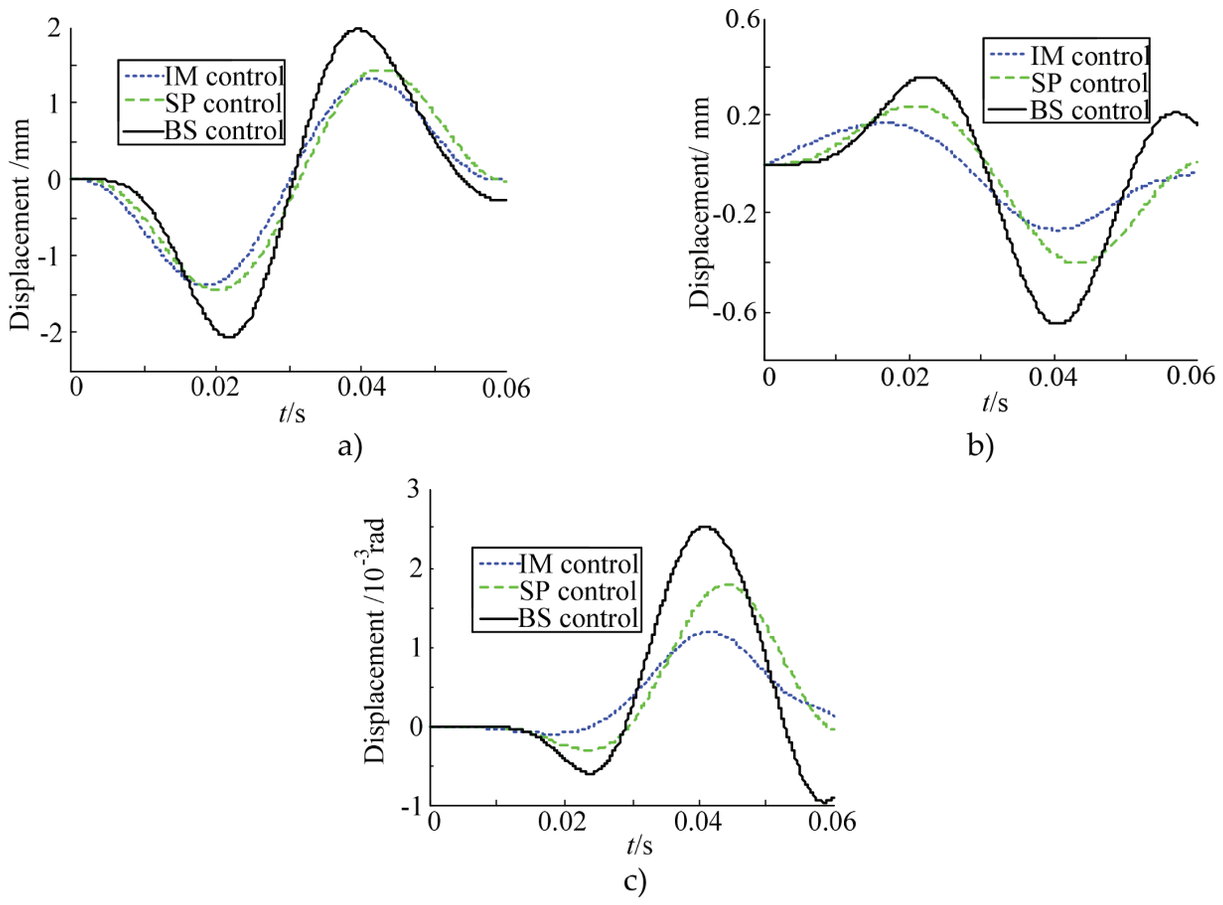

Figure 4. Flexible displacement of moving platform. (a) Displacement of X direction. (b) Displacement of Y direction. (c) Displacement of rotational direction.

http://dx.doi.org/10.5772/intechopen.80375

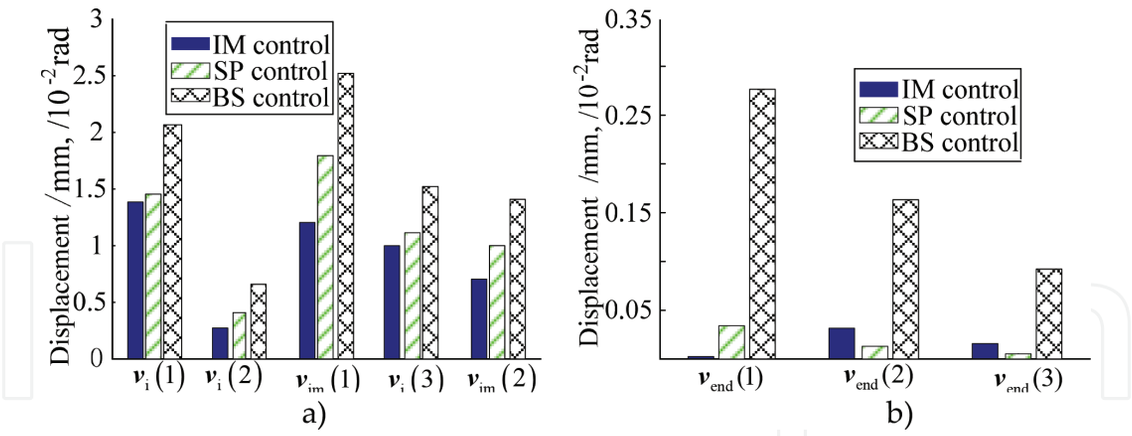

Figure 5. Vibration of the moving platform. (a) Flexible displacement of all directions. (b) Residue vibration of all directions.

The tracking error is the difference between the actual output and the desired output of the end of the moving platform. t_r indicates the maximum tracking error in all directions of the moving platform during the whole running process, t_{rm} indicates the average tracking error of the translational and rotational directions, t_{end} is the tracking error at the end point. As shown in **Figures 6** and **7**, compared with the singular perturbation and backstepping control,

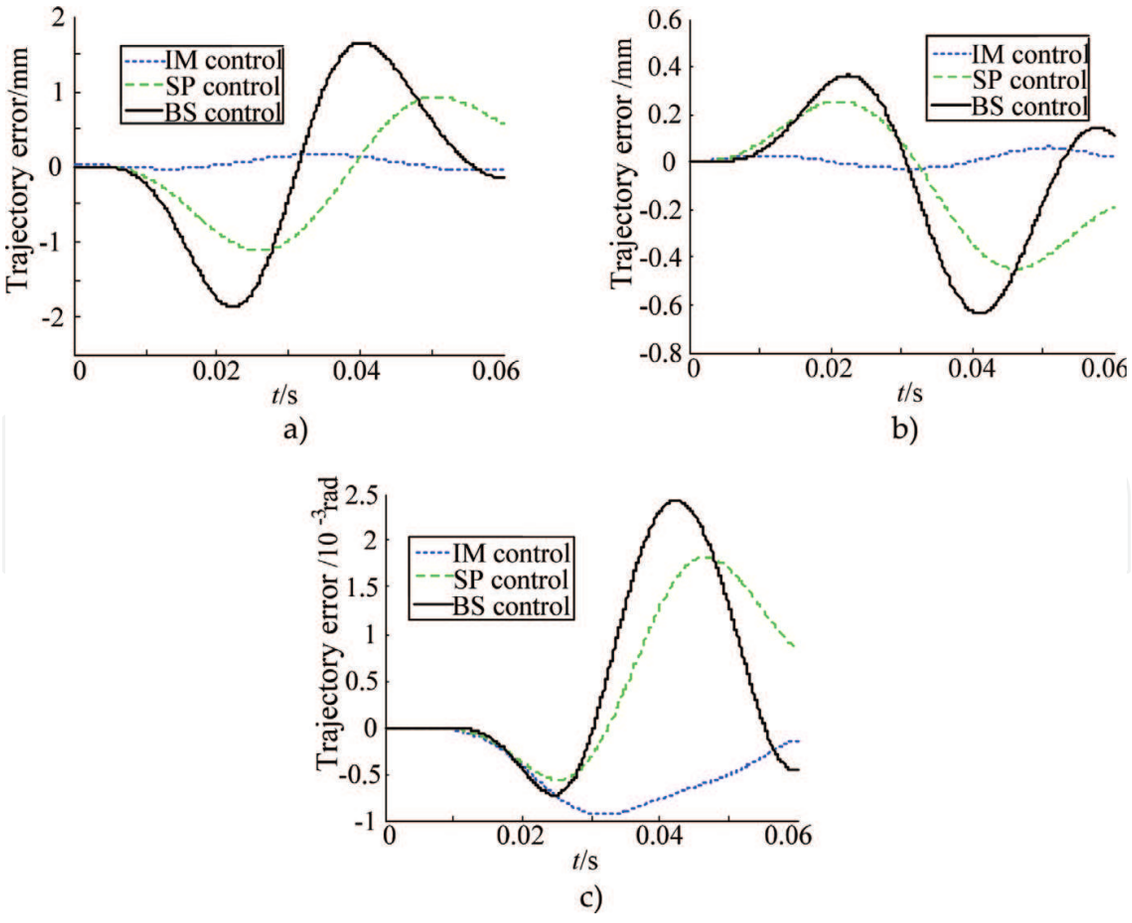

Figure 6. Trajectory error of directions. (a) Trajectory error of X direction. (b) Trajectory error of Y direction. (c) Trajectory error of rotational direction.

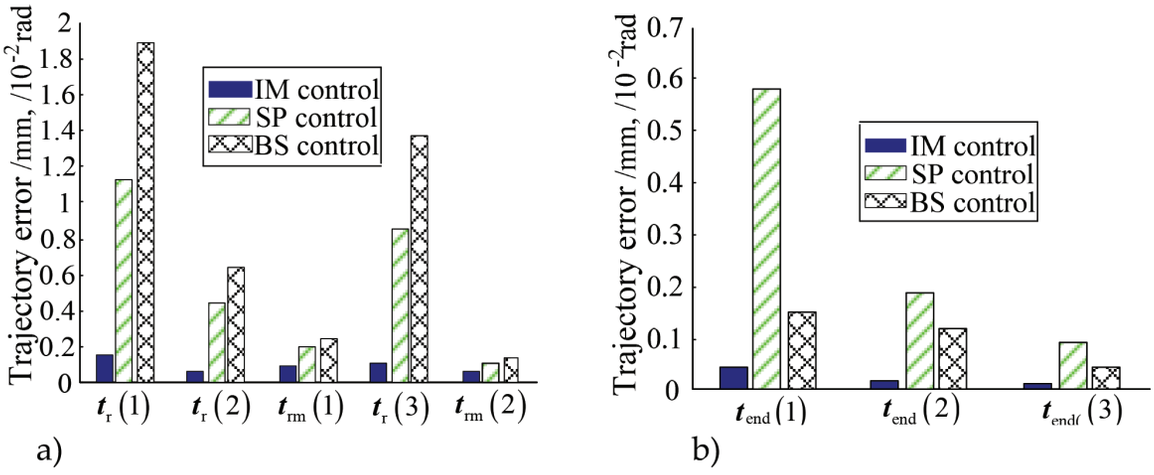

Figure 7. Tracking error of the moving platform. (a) Trajectory error of directions. (b) Residue error of directions.

the composite control based on the integral manifold and the observer has obvious advantages in trajectory tracking. For the maximum tracking error, the *X* direction decreased by 85.56 and 91.41%, and the *Y* direction decreased by 57.55 and 90.57%, while the rotation direction decreased by 53.34 and 61.5%, respectively. For the average tracking error, the translation direction decreased by 88.2 and 92.62%, the rotational direction decreased by 37.26 and 49.57%, respectively; in the tracking error of the end point, the *X* direction decreased by 92.8 and 72.34%, and the Y direction decreased by 89.73 and 83.62%, respectively, while the rotational direction decreased by 85.96 and 70.85%, respectively. For the tracking error at the end point, the singular perturbation method is significantly worse than the backstepping controller in all directions. This is mainly because the singular perturbation algorithm only considers the vibration suppression, and the cost of the vibration suppression is at the cost of sacrificing the trajectory tracking due to the delay of the adjustment. It can be seen from the above analysis that in the aspect of trajectory tracking accuracy, the composite control based on integral manifold and observer has significant advantages.

9. Conclusions

1. Decompose the rigid-flexible coupling dynamic model into fast and slow subsystems based on the integral manifold, and employ the sliding mode control and backstepping control to design the fast and slow subsystem controllers, respectively, and compensate the elastic displacement at the end of the manipulator. A high-gain observer estimates the rate of change of curvature, which in turn enables trajectory tracking control of high-speed PM.
2. The Lyapunov function is selected to prove the asymptotic stability of the slow subsystem, fast subsystem, high-gain observer, and the overall system. The conditions for selecting the integral manifold and the small parameters of the observer are given.
3. Apply MATLAB-SIMULINK to establish a comparison simulation to verify the performance of the proposed compound control algorithm. The simulation results show that the composite control algorithm has obvious advantages in vibration suppression and trajectory tracking.

Acknowledgements

This research was supported in part by the Natural Science Foundation of Zhejiang under Grant No. LY18E050019 and the Excellent Talent Cultivation Foundation under Grant No. ZSTUME02B09.

Author details

Zhengsheng Chen[1,2*]

*Address all correspondence to: zschen88200@163.com

1 School of Mechatronics Engineering, Harbin Institute of Technology, Harbin, China

2 Department of Mechatronics Engineering, Zhejiang Sci-tech University, Hangzhou, China

References

[1] Pietsch I, Krefft M, Becker O, et al. How to reach the dynamic limits of parallel robots? An autonomous control approach. IEEE Transactions on Automation Science and Engineering. 2005;**2**(4):369-380

[2] Dwivedy S, Eberhard P. Dynamic analysis of flexible manipulators, a literature review. Mechanism and Machine Theory. 2006;**41**(7):749-777

[3] Yongming LI, Tong S, Tieshan LI. Adaptive fuzzy output feedback control for a single-link flexible robot manipulator driven DC motor via backstepping. Nonlinear Analysis: Real World Applications. 2013;**14**(1):483-494

[4] Vakil M, Fotouhi R, Nikiforuk P. Causal end-effector inversion of a flexible link manipulator. Mechatronics. 2009;**19**(7):1197-1210

[5] Moallem M, Patel R, Khorasani K. Nonlinear tip-position tracking control of a flexible-link manipulator, theory and experiments. Automatica. 2001;**37**(11):1825-1834

[6] Lizarraga I, Etxebarria V. Combined PD-H_∞ approach to control of flexible link manipulators using only directly measurable variables. Cybernetics and Systems. 2003;**34**(1):19-31

[7] Zhang Q, Mills J, Cleghorn W, et al. Trajectory tracking and vibration suppression of a 3-PRR parallel manipulator with flexible links. Multibody System Dynamics. 2015;**33**(1): 27-60

[8] El-Badawy A, Mehrez MW, Ali AR. Nonlinear modeling and control of flexible-link manipulators subjected to parametric excitation. Nonlinear Dynamics. 2010;**62**(4):769-779

[9] Subudhi B, Morris A. Soft computing methods applied to the control of a flexible robot manipulator. Applied Soft Computing. 2009;**9**(1):149-158

[10] Khorasani K. Adaptive control of flexible-joint robots. IEEE Transactions on Robotics and Automation. 1992;**8**(2):250-267

[11] Moallem M, Khorasani K, Patel R. An integral manifold approach for tip-position tracking of flexible multi-link manipulators. IEEE Transactions on Robotics and Automation. 1997; **13**(6):823-837

[12] Salmasi H, Fotouhi R, Nikiforuk P. A manoeuvre control strategy for flexible-joint manipulators with joint dry friction. Robotica. 2010;**28**(04):621-635

[13] Vakil M, Fotouhi R, Nikiforuk P. Application of the integral manifold concept for the end-effector trajectory tracking of a flexible link manipulator. In: Proceedings of the 26th American Control Conference. New York: IEEE; 2007. pp. 741-747

[14] Vakil M, Fotouhi R, Nikiforuk P. End-effector trajectory tracking of a class of flexible link manipulators. In: Proceedings of 32nd Annual Mechanisms and Robotics Conference. New York: ASME; 2008. pp. 1085-1094

[15] Vakil M, Fotouhi R, Nikiforuk P. End-effector trajectory tracking of a flexible link manipulator using integral manifold concept. International Journal of Systems Science. 2011; **42**(12):2057-2069

[16] Vakil M, Fotouhi R, Nikiforuk P. Maneuver control of the multilink flexible manipulators. International Journal of Non-Linear Mechanics. 2009;**44**(8):831-844

[17] Chen Z, Kong M, Ji C, et al. An efficient dynamic modelling approach for high-speed planar parallel manipulator with flexible links. Proceedings of the Institution of Mechanical Engineers, Part C: Journal of Mechanical Engineering Science. 2015;**229**(4):663-678

[18] Gorius T, Seifried R, Eberhard P. Approximate end-effector tracking control of flexible multibody systems using singular perturbations. Journal of Computational and Nonlinear Dynamics. 2013;**9**(1):011017

[19] Ge Z, Lee T, Ge S. Tip tracking control of a single-link flexible robot, a backstepping approach. Dynamics and Control. 1997;**7**(4):341-360

[20] Lee S, Lee C. Hybrid control scheme for robust tracking of two-link flexible manipulator. Journal of Intelligent and Robotic Systems. 2001;**32**(4):389-410

[21] Heredia J, Wen Y. A high-gain observer-based PD control for robot manipulator. In: Proceedings of the 2000 American Control Conference. Chicago: IEEE; 2000. pp. 2518-2522

[22] Mosayebi M, Ghayour M, Sadigh M. A nonlinear high gain observer based input-output control of flexible link manipulator. Mechanics Research Communications. 2012;**45**:34-41